Computers and Structures 318 (2025) 107947

Contents lists available at ScienceDirect

Computers and Structures

journal homepage: www.elsevier.com/locate/cas

Active learning Kriging method based on particle swarm optimization for reliability analysis with random and interval hybrid uncertainty

Cheng Yang [a], Qingwei Liang [a,*], Hancheng Huang [a,b], Enrico Zio [b,c], Yuxin Lin [a], Shanshan Hu [a]

[a] College of Marine Science and Technology, Northwestern Polytechnical University, Xi'an, Shaanxi, 710072, PR China
[b] Centre for Research on Risk and Crises (CRC), Mines Paris-PSL University, Paris 75006, France
[c] Energy Department, Politecnico di Milano, Milano 20133, Italy

HIGHLIGHTS

- An adaptive Kriging reliability method is proposed for hybrid reliability analysis.
- The U-learning function is used to optimize the selection of optimal training samples.
- Search space reduction and domain truncation techniques are applied to enhance computational efficiency.
- An error-based stopping criterion is introduced to ensure the algorithm terminates appropriately.

ARTICLE INFO

Keywords:
Structural reliability
Random process
Interval uncertainty
Active learning
Kriging model
Error-based stopping criterion

ABSTRACT

We propose an active learning Kriging reliability method, based on the particle swarm optimization algorithm, to solve structural reliability assessment problems in which both random variables and parameter interval uncertainty coexist. The method optimizes the selection of optimal training samples by using the U learning function as the optimization objective, combined with search space reduction and domain truncation techniques. An error-based stopping criterion is employed to ensure termination of the algorithm. The effectiveness and feasibility of the proposed method are validated through five specific examples, whose results demonstrate the capability of the method to improve accuracy and computational efficiency in the reliability assessment.

1. Introduction

With the advancement of modern engineering technology, the complexity of structural design and construction continues to grow. Ensuring the safety and reliability of structures throughout their service life has become an important part of engineering design. Structural reliability refers to a structure's ability to maintain its intended functionality without failure under specified service life and environmental conditions, while bearing design loads and resisting environmental actions. Consequently, reliability analysis, as a critical link bridging design theory and engineering practice, is of fundamental importance. However, structural performance is inevitably influenced by various uncertainty factors, such as material properties, external loads, and manufacturing tolerances. A core challenge lies in precisely quantifying these uncertainties and accurately analyzing their impact on structural reliability in this field.

The quantification of uncertainty forms the foundation of reliability analysis. In current research, probabilistic models are widely adopted when sufficient statistical information is available, as they provide a rigorous framework for modeling random uncertainties. By representing uncertain parameters as random variables, various probabilistic reliability methods have been developed to analyze the failure probability of structures. The classic methods primarily include: 1) Monte Carlo Simulation (MCS) and its various improved versions [1,2]; and 2) analytical methods, such as the First-Order Reliability Method (FORM) and the Second-Order Reliability Method (SORM) [3–5]. While MCS is versatile, its prohibitive computational cost for problems involving small failure probabilities poses a significant limitation. FORM and SORM are computationally efficient, but their accuracy can be significantly compromised when the limit state function (LSF) exhibits high nonlinearity or involves multiple failure modes. To balance accuracy and efficiency,

* Corresponding author.
Email address: liangqingwei@nwpu.edu.cn (Q. Liang).

https://doi.org/10.1016/j.compstruc.2025.107947
Received 5 May 2025; Accepted 31 August 2025
Available online 11 September 2025

active learning methods based on surrogate models have been extensively studied. These methods significantly improve analysis efficiency by adaptively selecting new sample points [6–10].

However, in many practical engineering problems, obtaining precise probability distributions for uncertain parameters is extremely challenging, especially when experimental data are scarce or during the early design stages. In such data-deficient scenarios, non-probabilistic models provide a more practical alternative. Among these non-probabilistic approaches, the interval model characterizes uncertainty by specifying only the upper and lower bounds of parameters, thereby enabling reliability analysis when probabilistic information is insufficient or unavailable. On the basis of interval modeling, various non-probabilistic reliability theories have been developed, such as evidence theory [11–13] and grey system theory [14]. Although these methods relax the requirements for input information, they cannot fully utilize the information from parameters that possess well-defined probabilistic characteristics, and their analysis results may sometimes be overly conservative. Therefore, to more comprehensively and realistically describe complex systems where both types of uncertainties coexist, the study of hybrid uncertainty models that combine random and interval representations has become particularly necessary and urgent.

As a result, hybrid reliability analysis (HRA) has emerged as an active research area in recent years for addressing such problems [15–20]. HRA inherently involves a nested process of probabilistic and interval analysis. Direct solutions often rely on Monte Carlo Simulation (MCS), but the associated high computational cost renders this approach impractical for large-scale numerical simulations, such as finite element analysis. To overcome this bottleneck, several alternative approaches have been proposed. For example, Du et al. [21] introduced a unified reliability analysis method based on FORM, termed FORM-UUA. Xiao et al. [22] proposed a mean first-order saddle point approximation method, which utilizes first-order Taylor series linearization to efficiently determine the extreme values of the response. However, for problems involving highly nonlinear functions or multiple design points, the computational accuracy of these methods may not be guaranteed. To address these limitations, researchers have actively explored various efficient alternatives, among which surrogate model-based active learning strategies have emerged as the most flexible and widely adopted approach [23–28]. Within this framework, the research focus is on efficiently generating and evaluating potential sample points to accurately identify the true failure boundary with minimal computational cost. Current studies primarily address two critical aspects: first, the optimization of candidate sample generation strategies. Traditional methods relying on large-scale sampling pools are inefficient; thus, a significant research direction is the design of more efficient sampling spaces to reduce the scope of the candidate pool [29]. The second aspect is the refinement of the mechanisms for evaluating and utilizing sample points [30]. Most methods design various active learning functions to evaluate the importance of candidate points. For example, Yang et al. [31] developed an active learning Kriging method for HRA (ALK-HRA). However, in the ALK-HRA method, the Kriging model is trained to approximate the entire limit-state surface involving both random and interval inputs, which may result in computational inefficiency. Based on the relationship between the bounds of the LSS projected onto the random space and the bounds of the failure probability, Zhang et al. [32–34] proposed a projection-outline-based active learning Kriging method (POALK). Nevertheless, POALK may not always exhibit robust or efficient performance when addressing complex problems. Drawing inspiration from system reliability, Yang et al. [35] proposed a truncated candidate region HRA method based on active learning Kriging (ALK-TCR-HRA). Although this-method is robust and effective, its candidate sample pool can become excessively large, particularly in problems involving small failure probabilities. Xiao et al. [36] combined subset simulation with active learning Kriging to propose a hybrid reliability analysis method for problems with random and interval variables. Zhao et al. [37] further proposed a novel random and interval reliability analysis approach by combining active learning Kriging with two-stage subset simulation.

Despite the significant progress achieved by the aforementioned active learning HRA methods through the continuous optimization of candidate point generation and evaluation mechanisms, there remains room for improvement in their overall adaptive learning strategies. Existing methods typically operate within a fixed framework, employing a learning function in a predetermined manner to select the next optimal sample point from a large pool of candidates. This approach may not fully exploit the potential of the learning function, particularly in complex hybrid problems. To address this limitation, this paper proposes a novel adaptive Kriging method. The core of the proposed method is the development of a comprehensive adaptive learning strategy, which aims to eliminate the dependence on limited candidate sample pools in traditional methods, thus enabling more efficient and globally optimized sample point selection. The main innovations of this work are summarized as follows:

1. Global adaptive sampling: Particle swarm optimization (PSO) is employed to perform a global search during the sampling process, thereby eliminating the dependence on limited candidate sample pools. This enables adaptive selection of optimal new samples throughout the entire sample space, enhancing the representational capability and sampling efficiency of the Kriging model.
2. Search space constraints and truncation: By introducing search space reduction and regional truncation techniques, the optimization efficiency is further improved, which ensures the feasibility and efficiency of the global sampling strategy in high-dimensional and complex systems.
3. Hybrid uncertainty extension for the error-based stopping criterion (ESC): The ESC is systematically extended to stochastic-interval hybrid uncertainty problems, thereby enabling adaptive and efficient convergence assessment for maximum/minimum failure probability intervals and broadening the applicability of the ESC.

The remainder of the paper is organized as follows. Section 2 introduces the fundamentals of HRA and the Kriging model. Section 3 details the proposed method and stopping criterion. Section 4 presents the implementation steps of the proposed method. Section 5 validates the proposed reliability analysis method through five specific examples. Finally, Section 6 concludes the paper.

2. Basic theory

This-section establishes the theoretical groundwork necessary for understanding the proposed method. It begins by presenting the mathematical formulation of the HRA problem, defining how the interaction between random and interval variables leads to the generation of failure probability bounds. Subsequently, the principles of the Kriging model for constructing a surrogate of the LSF are detailed. These foundational concepts are central to the adaptive learning strategy developed in the following chapters.

2.1. Basics of HRA

For HRA involving both random and interval variables, the relationship between structural performance and the uncertainties is described by the LSF, denoted as $G(\boldsymbol{X},\boldsymbol{Y})$. In this function, $\boldsymbol{X}=[x_1,x_2,\ldots,x_n]^T$ is the n-dimensional vector of random variables, and $\boldsymbol{Y}=[y_1,y_2,\ldots,y_m]^T$ is the m-dimensional vector of interval variables. Each component y_i of the interval vector is an interval defined by its lower and upper bounds, $y_i=[y_i^L,Y_i^U]$. The set of all possible realizations of $\boldsymbol{Y}$ constitutes a hyper-rectangular domain $[\boldsymbol{Y^L},\boldsymbol{Y^U}]$, bounded by the lower-bound vector $\boldsymbol{Y^L}=[y_1^L,y_2^L,\ldots,y_m^L]$ and the upper-bound vector $\boldsymbol{Y^U}=[y_1^U,y_2^U,\ldots,y_m^U]$ [27,28]. The existence of interval variables results in the

failure probability being characterized as a range rather than a single deterministic value. The lower and upper bounds of the failure probability, P_f^{min} and P_f^{max}, are given by Eqs. (1) and (2), respectively:

$$p_f^{\max} = P\left\{\min_{\mathbf{Y}\in[\mathbf{Y}^L,\mathbf{Y}^U]} G(\mathbf{X},\mathbf{Y}) \le 0\right\} = E\left[I_F\left(\min_{\mathbf{Y}\in[\mathbf{Y}^L,\mathbf{Y}^U]} G(\mathbf{X},\mathbf{Y}) \le 0\right)\right] \tag{1}$$

$$p_f^{\min} = P\left\{\max_{\mathbf{Y}\in[\mathbf{Y}^L,\mathbf{Y}^U]} G(\mathbf{X},\mathbf{Y}) \le 0\right\} = E\left[I_F\left(\max_{\mathbf{Y}\in[\mathbf{Y}^L,\mathbf{Y}^U]} G(\mathbf{X},\mathbf{Y}) \le 0\right)\right] \tag{2}$$

where $P\{\cdot\}$ is the probability operator, $I_F(\cdot)$ is the failure indicator function, and $E[\cdot]$ represents the expectation operator. The primary objective of HRA is to compute these failure probability bounds.

Using the MCS, the failure probability can be approximated as follows:

$$\hat{p}_f^{\max} = \frac{1}{N_{MC}}\sum_{j=1}^{N_{MC}} I_F\left(\min_{\mathbf{Y}\in[\mathbf{Y}^L,\mathbf{Y}^U]} G(\boldsymbol{X}^{(j)},\boldsymbol{Y}) < 0\right) \tag{3}$$

$$\hat{p}_f^{\min} = \frac{1}{N_{MC}}\sum_{j=1}^{N_{MC}} I_F\left(\max_{\mathbf{Y}\in[\mathbf{Y}^L,\mathbf{Y}^U]} G(\boldsymbol{X}^{(j)},\boldsymbol{Y}) < 0\right) \tag{4}$$

where $\boldsymbol{X}^{(j)}(j = 1, 2, \ldots, N_{MC})$ denotes the generic $j-th$ sample generated through MCS. The coefficients of variation (Cov) are given by:

$$Cov(\hat{p}_f^{\max}) = \sqrt{\frac{1-\hat{p}_f^{\max}}{N_{MC}\hat{p}_f^{\max}}} \tag{5}$$

$$Cov(\hat{p}_f^{\min}) = \sqrt{\frac{1-\hat{p}_f^{\min}}{N_{MC}\hat{p}_f^{\min}}} \tag{6}$$

2.2. Kriging model

The Kriging surrogate model is a statistical method widely used in surrogate modeling. Compared to other interpolation techniques, Kriging offers two primary advantages: It only requires information from points near the estimation location when approximating unknown quantities; Due to its combined local and global statistical properties, it is capable of predicting trends and dynamics of the system. A general Kriging model consists of two components: a regression component and a stochastic component [38]. Based on k n-dimensional sample points and their corresponding response values $G(\boldsymbol{d})$, the Kriging surrogate model can be expressed as:

$$G(\boldsymbol{d}) = f^T(\boldsymbol{d})\beta + Z(\boldsymbol{d}) \tag{7}$$

where $f(\boldsymbol{d}) = [f_1(\boldsymbol{d}), f_2(\boldsymbol{d}), \ldots, f_m(\boldsymbol{d})]^T$ denotes a vector comprising m basis functions; and $\beta = [\beta_1, \beta_2, \ldots, \beta_m]^T$ is an m-dimensional vector of regression coefficients. The term $Z(\boldsymbol{d})$ is a stationary Gaussian process with a mean of zero and a variance of σ^2, whose covariance is defined as:

$$Cov(Z(d_i), Z(d_j)) = \sigma^2 R(d_i, d_j)\ (i, j = 1, 2, \ldots, k) \tag{8}$$

Between two sample points d_i and d_j, the spatial correlation function $R(d_i, d_j)$ can be defined using various forms, such as exponential, Matérn, and spherical functions. In this study, we adopt the Gaussian correlation function, which is expressed as:

$$R(d_i, d_j) = \exp\left[-\sum_{l=1}^{k}\theta_l(d_{i,l} - d_{j,l})^2\right] \tag{9}$$

where $d_{i,l}$ represent the $l-th$ components of the vectors d_i. The correlation parameters θ_l are derived using maximum likelihood estimation. The expression for the log-likelihood function is given by:

$$\ln[L(\boldsymbol{\theta})] = -\frac{1}{2}\ln(|R|) - \frac{k}{2}\ln\left(\sigma^2\right) + C \tag{10}$$

where $R = [R_{ij}]_{k\times k}$ is the correlation matrix with $R_{ij} = R(d_i, d_j)(i, j = 1, 2, \ldots, k)$, and C is a constant. The correlation parameters θ can be obtained by solving the following optimization problem:

$$\min\left\{\frac{1}{2}\ln(|R|) + \frac{k}{2}\ln\left(\sigma^2\right)\right\} \tag{11}$$

Using the least squares method, the regression coefficients $\hat{\beta}$ and the variance of the Gaussian process $\hat{\sigma}^2$ can be estimated as:

$$\hat{\beta} = \left(F^T R^{-1} F\right)^{-1} F^T R^{-1} G \tag{12}$$

$$\hat{\sigma}^2 = \frac{1}{k}(G - F\hat{\beta})^T R^{-1}\left(G - F\hat{\beta}\right) \tag{13}$$

where $F = [F_{ij}]_{k\times m}$, $F_{ij} = f_j(d_i)(i = 1, 2, \ldots, k,\ j = 1, 2, \ldots, m)$.

For any arbitrary unknown point d_0, the predicted response $\hat{G}(d_0)$ follows a normal distribution $N(\mu_{\hat{G}}(d_0), \sigma^2_{\hat{G}}(d_0))$. The best linear unbiased prediction $\mu_{\hat{G}}(d_0)$ and its mean squared error $\sigma^2_{\hat{G}}(d_0)$ can be expressed as:

$$\mu_{\hat{G}}(d_0) = f^T(d_0)\hat{\beta} + r_0^T R^{-1}\left(G - F\hat{\beta}\right) \tag{14}$$

$$\sigma^2_{\hat{G}}(d_0) = \sigma^2(1 + u^T)\left(F^T R^{-1} F\right)^{-1} u - r_0^T R^{-1} r_0 \tag{15}$$

where $r_0 = [R(d_0, d_1), R(d_0, d_2), \ldots, R(d_0, d_k)]^T$ is the covariance matrix of the correlation vector among the prediction point d_0 and all k sample points $d_1, d_2, \ldots, d_k$, $u = F^T R^{-1} r_0 - f(d_0)$. The variance $\sigma^2_{\hat{G}}(d_0)$ is often used to evaluate the prediction error at d_0, and it also serves as the foundation for active learning methods.

3. Adaptive Kriging algorithm based on PSO

This-section presents the core methodological contribution of this study: a novel adaptive learning strategy designed for the efficient and global exploration of the failure region. It elaborates on the strategy for defining both the objective learning function and the adaptive search space constraints. Furthermore, the ESC is described and adapted for the hybrid reliability context to ensure the simulation terminates adaptively and efficiently.

3.1. Determination of the objective function

In the process of estimating failure probability, it is necessary to repeatedly evaluate the true performance function, which is typically represented by a high-fidelity numerical model (such as finite element analysis or other complex simulations). Each evaluation of such a model is computationally intensive, and the large number of required evaluations—often on the order of thousands or more for methods like MCS—results in a substantial overall computational cost. Therefore, the active learning Kriging model is introduced in HRA as a surrogate. Typically, various learning functions such as the Expected Risk Function (ERF) [6] and U learning function [7] are applied to identify the most effective training points for refining the Kriging model. In this study, the U learning function was selected because it effectively balances exploration and exploitation by considering both the predicted response and prediction uncertainty [35]. This makes it particularly suitable for reliability problems with mixed uncertainties, as it efficiently identifies samples near the limit state boundary where prediction accuracy is most critical.

$$U_{learn}(\boldsymbol{X},\boldsymbol{Y}) = \frac{|\mu_G(\boldsymbol{X},\boldsymbol{Y})|}{\sigma_G(\boldsymbol{X},\boldsymbol{Y})} \tag{16}$$

Since all optimization calculations in this study are carried out in the standard normal space, the random variables $\boldsymbol{X}$ are transformed into independent standard normal variables $\boldsymbol{U}$ using either the iso-probability

transformation or the $Nataf$ transformation. Thus, the LSF with both random and interval variables is described as $G(\boldsymbol{U},\boldsymbol{Y})$. Consequently, the optimization objective function is reformulated as:

$$[\boldsymbol{U},\boldsymbol{Y}] = \arg\min \frac{\left|\mu_G(\boldsymbol{U},\boldsymbol{Y})\right|}{\sigma_G(\boldsymbol{U},\boldsymbol{Y})} \tag{17}$$

3.2. Determination of constraints

3.2.1. Distance constraint

In the computation of HRA, selecting new sample points requires consideration of the potential risk of clustering among the random variable samples. Accordingly, distance criterion is adopted to ensure that the optimal new sample point for random variables is sufficiently distant from the existing sample points: this is necessary to avoid overfitting the Kriging model. The distance function is defined as [39]:

$$d_{\min} = \min_i \sqrt{(\boldsymbol{U}-\boldsymbol{U_i})^T(\boldsymbol{U}-\boldsymbol{U_i})} < \delta \tag{18}$$

where $\boldsymbol{U_i}$ represents the random variable portion of the sample point, and $d_{\min}$ is the minimum Euclidean distance between $\boldsymbol{X}$ and the existing training samples. δ is a threshold determined based on practical engineering problems: in this study, a recommended value of $\delta = 0.01$ is adopted based on empirical experience. The primary role of the distance threshold δ is to ensure good space-filling properties of the samples and to maintain the numerical stability of the Kriging model. The recommended value is an empirically robust choice. It is small enough not to overly constrain the optimization process, yet large enough to effectively prevent the Kriging correlation matrix from becoming ill-conditioned or singular due to excessively close sample points. This, in turn, prevents model overfitting and ensures the robustness of the algorithm. Note that all constraints in this-section apply exclusively to the random variable portion of the sample points.

3.2.2. Search space constraints

To accelerate the optimization process, the search space is restricted to a hypersphere region [29,40]. It is defined as the region between the outer radius β_1 and inner radius β_2, as shown in Eq. (19) and Fig. 1:

$$\beta_2 \leqslant \|\boldsymbol{U}\|_2 \leqslant \beta_1 \tag{19}$$

where $\|.\|_2$ denotes the ℓ_2-norm.

First, the inner radius β_2 is predefined based on a reliability standard. The parameters β_2 and β_1 are used to define a region of interest $[\beta_2, \beta_1]$

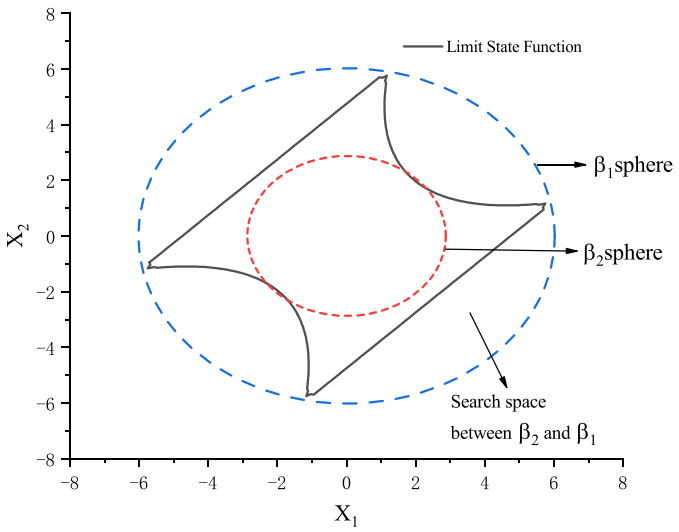

Fig. 1. Search space.

that conforms to engineering practice, in order to focus computational resources on the most valuable samples. The core role of β_2 is to improve computational efficiency, and its principle is to actively exclude the high-probability safe region. In the standard normal space, the probability density is highest at the origin. $\beta_2 = 1$ defines a hypersphere with a radius of 1. The sample points within this region can almost certainly be considered safe (their one-sided failure probability is greater than $\Phi(-1) \approx 15.9\ \%$), and their contribution to the final failure probability is negligible. Therefore, we recommend $\beta_2 = 1$ in order to concentrate computational resources on the critical regions where failure is more likely to occur.

Secondly, the adaptive outer radius β_1 is updated adaptively through Eq. (20), thereby dynamically shrinking or expanding the search range for the next iteration.

$$\beta_1 = \begin{cases} \varepsilon & \alpha_1 R_{AMPP} > \varepsilon \\ \alpha_1 R_{AMPP} & \alpha_1 R_{AMPP} < \varepsilon \end{cases} \tag{20}$$

where R_{AMPP} is defined as the minimum value among the distances from each sample in the current training set to the LSS along its radial direction. α_1 is the scaling factor for R_{AMPP}, and ε serves as the upper threshold for the algorithm's exploration range.

The scaling factor α_1 is used to dynamically adjust the search radius to balance the exploration of unknown regions and the exploitation of the known boundary. This paper recommends a value of $\alpha_1 = \sqrt{2}$. This is justified from a geometric perspective: if a square is inscribed within a circular failure boundary, the radius of the circumscribing circle is $\sqrt{2}$ times the distance from the origin to a vertex of the square. This implies that if we treat the current R_{AMPP} as the distance to a vertex of such an inscribed square, multiplying it by $\sqrt{2}$ expands the search radius to cover the circumscribed circle containing that square. Geometrically, this-provides a reasonable scale for expanding from a "point" to a "surface," facilitating the exploration of the unknown regions surrounding R_{AMPP}. From a probabilistic perspective, increasing the search radius from a value β to $\sqrt{2}\beta$ allows the algorithm to span an order of magnitude in the probability space, which is crucial for efficiently locating small probability events.

Simultaneously, ε sets a practical upper limit on the algorithm's exploration range to avoid unnecessary computations. We recommend $\varepsilon = 5.6$, as this-value is directly derived from an analysis of reliability indices for common engineering structures. The failure probability for typical structures usually ranges from 10^{-1} to 10^{-8}, and a P_f of 10^{-8} corresponds to a reliability index β of approximately 5.61. By setting ε to 5.6, the algorithm's search range can fully cover the reliability levels of interest for the vast majority of engineering problems.

Another key value for determining β_1 is R_{AMPP}. Its specific calculation process is as follows:

(1) Determine the target LSS: For any random variable sample U in the current training set, the corresponding limit state surface must first be identified. In handling problems with mixed random and interval variables, the limit state is not a single surface but a region determined by the interval variables Y. To ensure the completeness of the search—thereby effectively avoiding the omission of important failure modes and guaranteeing the algorithm's convergence and accuracy—we must consider the outermost potential failure boundary. This corresponds to the "best-case" limit state, which is found by identifying the combination of interval variables, $Y_{\max}$, that maximizes the performance function $G(U_i, Y)$ via an optimization process, as shown in Eq. (21).

$$\boldsymbol{Y}_{\max} = \arg\max G(\boldsymbol{U},\boldsymbol{Y}),\ \boldsymbol{Y} \in [\boldsymbol{Y}^{\boldsymbol{L}}, \boldsymbol{Y}^{\boldsymbol{U}}] \tag{21}$$

(2) Find the approximate most probable point (AMPP): Once the target surface is determined, a line is constructed from the origin through the point $[U, Y_{\max}]$. An AMPP candidate is defined as a location on this line where the Kriging surrogate model's prediction is zero, i.e., $\hat{G}(U, Y_{\max}) = 0$, as illustrated in Fig. 2. To find all AMPP candidates

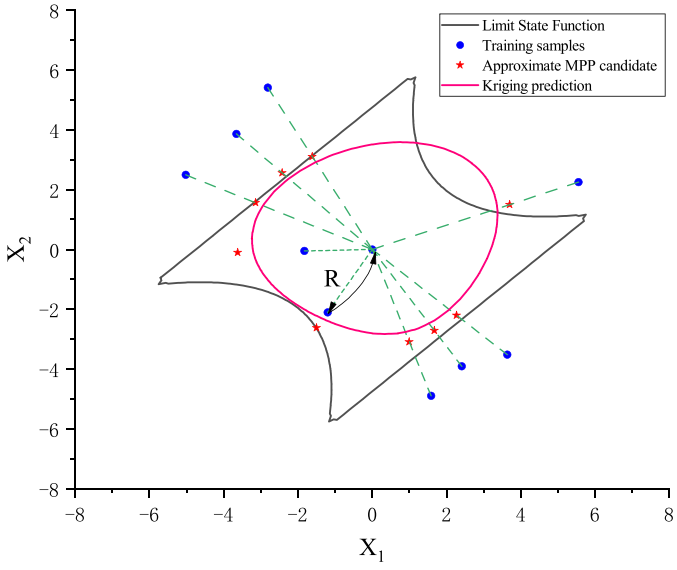

Fig. 2. Line search.

for a given sample, a radial search is performed. If the sample is located in the failure region ($\hat{G}(U, Y_{\max}) \leqslant 0$), the radial distance r is decreased in steps of Δr, and the new point $[U_{new}, Y_{\max}]$ is evaluated until an AMPP candidate is found. Conversely, if the sample is in the safe region ($\hat{G}(U, Y_{\max}) > 0$), the radial distance is increased by increments of Δr. The parameter Δr defines the discrete step size for the radial search along the LSF, representing a trade-off between positioning accuracy and computational efficiency. In this study, we recommend $\Delta r = 0.1$, a value that has been empirically verified to maintain high computational efficiency while ensuring sufficient accuracy. It is noteworthy that the algorithm's adaptive learning mechanism exhibits robustness to the choice of Δr. Any minor inaccuracies in AMPP localization caused by the discrete step size can be compensated for in subsequent iterations, as the scaling factor α_1 dynamically adjusts the global search radius, thereby mitigating the impact of the initial discretization.

(3) Calculate R_{AMPP}: After identifying all AMPP candidates generated from the entire training set, R_{AMPP} is defined as the minimum distance from the origin among all these candidates. If no AMPP candidates are found for any sample (e.g., all samples are located far from the boundary in the safe region), R_{AMPP} is assigned a default value, for instance, 3.

3.2.3. Truncated domain constraint

As shown in Fig. 3, the projection of $G(\boldsymbol{U}, \boldsymbol{Y}) = 0$ into the random variable domain forms a strip-shaped region. If the U learning function is directly used to choose the most suitable training points, these points may lie within the strip-shaped region. However, only the boundaries of the region $\min_{j=1}^{N_y} G(\boldsymbol{U}, \boldsymbol{Y}^{(j)})$ and $\max_{j=1}^{N_y} G(\boldsymbol{U}, \boldsymbol{Y}^{(j)})$ determine the bounds of the failure rates, P_f^{max} and P_f^{min}, respectively. Therefore, it is expected that constraining the training points to lie near the boundaries of the strip-shaped region will reduce the number of function evaluations without sacrificing accuracy. In this study, the truncated domain constraint P_f^{max} is expressed as [35]:

$$\tilde{\Omega}_{\min}(\boldsymbol{U}) = \left\{ \boldsymbol{U} \,|\, \min_{j=1}^{N_y} \left[\mu_G(\boldsymbol{U}, \boldsymbol{Y}^{(j)} + 2\sigma_G(\boldsymbol{U}, \boldsymbol{Y}^{(j)}) \right] > 0 \right\} \tag{22}$$

and P_f^{min}:

$$\tilde{\Omega}_{\max}(\boldsymbol{U}) = \left\{ \boldsymbol{U} \,|\, \max_{j=1}^{N_y} \left[\mu_G(\boldsymbol{U}, \boldsymbol{Y}^{(j)} - 2\sigma_G(\boldsymbol{U}, \boldsymbol{Y}^{(j)}) \right] < 0 \right\} \tag{23}$$

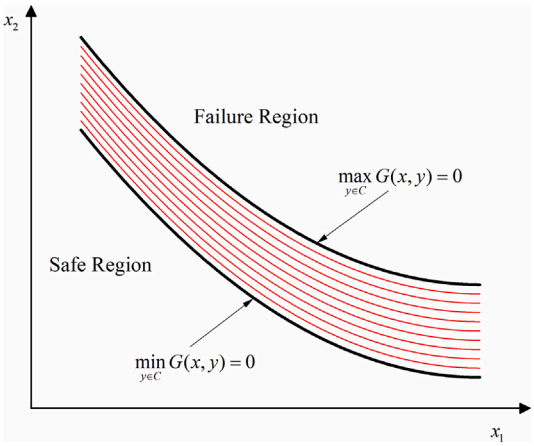

Fig. 3. Projection of the LSS into a two-dimensional random domain.

Combining Eqs. (16)–(23), the final optimization function is expressed as:

$$\begin{aligned} &obj \;\; \arg\min \frac{|\mu_G(\boldsymbol{U}, \boldsymbol{Y})|}{\sigma_G(\boldsymbol{U}, \boldsymbol{Y})} \\ &s.t. \; d_{\min} < \delta \\ &\quad \beta_2 \leqslant \|\boldsymbol{U}\|_2 \leqslant \beta_1 \\ &\quad \tilde{\Omega}_{\min}(\boldsymbol{U}) \; or \; \tilde{\Omega}_{\max}(\boldsymbol{U}) \end{aligned} \tag{24}$$

In this study, the optimization of the objective function is performed using MATLAB's built-in *particleswarm* function. To ensure that the research focus remains on evaluating the effectiveness of the proposed adaptive sampling framework, rather than on parameter tuning of the optimizer, we adopted the function's well-validated default parameter settings. These standardized parameters provide a robust and reproducible benchmark for the algorithm's performance.

3.3. Stopping criterion

Besides the aforementioned optimized sampling scheme, the stopping criterion for the active learning process is a crucial component in establishing an adaptive method based on Kriging. Generally, setting a threshold for the learning function is the most widely used convergence criterion, but this approach can sometimes be overly conservative, leading to unnecessary calls to the performance function and increased computational cost. To address this issue, this paper introduces the ESC as the adaptive termination criterion for the algorithm. The ESC, which is based on the precision of the failure probability estimation, has demonstrated superior performance in numerous instances [41–43].

The relative error between the predicted failure rate $\hat{p}_f$ by the surrogate Kriging model and the actual failure rate results p_f can be approximated as follows:

$$\varepsilon_r = \left| \frac{p_f - \hat{p}_f}{p_f} \right| \approx \left| \frac{p_f^{MCS} - \hat{p}_f}{p_f^{MCS}} \right| = \left| \frac{\frac{N_f}{N_{MCS}} - \frac{\hat{N}_f}{N_{MCS}}}{\frac{N_f}{N_{MCS}}} \right| = \left| \frac{\hat{N}_f}{N_f} - 1 \right| \tag{25}$$

where p_f^{MCS} is the failure probability calculated via the MCS method, N_{MCS} represents the number of candidate design sample points used in the MCS method, N_f denotes the number of failure samples determined by evaluating the true limit state function, and $\hat{N}_f$ is the number of failure samples identified by the Kriging surrogate model.

For the calculation of N_f, the following equation is employed:

$$N_f = \hat{N}_f + \hat{N}_{sf} - \hat{N}_{fs} \tag{26}$$

where $\hat{N}_{fs}$ represents the number of candidate sample points $\hat{\Omega}_f$ within the failure domain that are misclassified by the Kriging model, and $\hat{N}_{sf}$

represents the number of candidate sample points $\hat{\Omega}_s$ within the safe domain that are incorrectly predicted as safe samples by the Kriging model.

Given the Gaussian properties of the Kriging model predictions, the probability of a sign error in the performance function value at any candidate sample $\boldsymbol{X}_i$ is denoted as $p(\boldsymbol{X}_i)$:

$$p(\boldsymbol{X}_i) = \Phi\left(-\left|\frac{\hat{\mu}_{\hat{g}}(\boldsymbol{X}_i)}{\hat{\sigma}_{\hat{g}}(\boldsymbol{X}_i)}\right|\right) \tag{27}$$

Using an indicator function I_{Wi}, the result of the Kriging model's prediction of the symbols in the candidate sample $\boldsymbol{X}_i$ can be represented. When the Kriging model incorrectly predicts the symbol in $\boldsymbol{X}_i$, the indicator function $I_{Wi} = 1$, otherwise $I_{Wi} = 0$. In this case, I_{Wi} is a Bernoulli random variable with an expectation and variance of $p(\boldsymbol{X}_i)$ and $p(\boldsymbol{X}_i)(1 - p(\boldsymbol{X}_i))$, respectively. Based on the definitions of $\hat{N}_{sf}$ and $\hat{N}_{fs}$, the following relationships can be derived:

$$\hat{N}_{sf} = \sum_{i=1}^{\hat{N}_s} I_{Wi},\ \boldsymbol{X}_i \in \hat{\Omega}_s \tag{28}$$

$$\hat{N}_{fs} = \sum_{i=1}^{\hat{N}_f} I_{Wi},\ \boldsymbol{X}_i \in \hat{\Omega}_f \tag{29}$$

where $\hat{\Omega}_s$ and $\hat{\Omega}_f$ represent the failure and safe domains, respectively. $\hat{N}_s$ and $\hat{N}_f$ denote the number of candidate samples in these domains.

Since the sum of independent Bernoulli trials follows a Poisson-binomial distribution, both $\hat{N}_s$ and $\hat{N}_f$ also follow such a distribution, and thus $\hat{N}_{sf} \sim pb(\mu_{\hat{N}_{sf}}, \sigma^2_{\hat{N}_{sf}})$ and $\hat{N}_{fs} \sim pb(\mu_{\hat{N}_{fs}}, \sigma^2_{\hat{N}_{fs}})$ whose parameters can be expressed as:

$$\mu_{\hat{N}_{sf}} = \sum_{i=1}^{\hat{N}_s} p(\boldsymbol{X}_i)\ \sigma^2_{\hat{N}_{sf}} = \sum_{i=1}^{\hat{N}_s} p(\boldsymbol{X}_i)(1 - p(\boldsymbol{X}_i)) \tag{30}$$

$$\mu_{\hat{N}_{fs}} = \sum_{i=1}^{\hat{N}_f} p(\boldsymbol{X}_i)\ \sigma^2_{\hat{N}_{fs}} = \sum_{i=1}^{\hat{N}_f} p(\boldsymbol{X}_i)(1 - p(\boldsymbol{X}_i)) \tag{31}$$

The confidence interval for N_f at a confidence level of α, based on Eq. (26), can be expressed as [41]:

$$N_f \in \left[\hat{N}_f - \hat{N}^u_{fs}, \hat{N}_f + \hat{N}^u_{sf}\right] \tag{32}$$

where $\hat{N}^u_{fs}$ and $\hat{N}^u_{sf}$ are the critical values corresponding to the confidence level of $\hat{N}_{fs}$ and $\hat{N}_{sf}$, respectively.

For the quantification of $\hat{N}^u_{fs}$ and $\hat{N}^u_{sf}$, the approximation methods proposed in the literature [43] are adopted:

$$\hat{N}^u_{fs} = \mu_{\hat{N}_{fs}} + 3\sigma_{\hat{N}_{fs}} \tag{33}$$

$$\hat{N}^u_{sf} = \mu_{\hat{N}_{sf}} + 3\sigma_{\hat{N}_{sf}} \tag{34}$$

Combining Eq. (26) through (34), the ESC for the proposed method can be established as:

$$\varepsilon_r \leqslant \max\left(\left|\frac{\hat{N}_f}{\hat{N}_f - \hat{N}^u_{fs}} - 1\right|, \left|\frac{\hat{N}_f}{\hat{N}_f + \hat{N}^u_{sf}} - 1\right|\right) = \hat{\varepsilon}_{\max ESC} \leqslant \varepsilon_{tol} \tag{35}$$

For the assessment of hybrid reliability, the stopping criterion can be further constructed as:

$$\varepsilon_{HRA} = \max(\varepsilon_r^{P_f^{max}}, \varepsilon_r^{P_f^{min}}) < \varepsilon_{tol} \tag{36}$$

where ε_{tol} is the prescribed threshold for the relative error of the failure probability estimate, recommended to be 0.001 in this work [41]. $\varepsilon_r^{P_f^{max}}$ is is the relative error of P_f^{max} and $\varepsilon_r^{P_f^{min}}$ is the relative error of P_f^{min}.

4. Implementation steps of the proposed method

Building upon the theoretical and methodological foundations established in Sections 2 and 3, this-section outlines the comprehensive step-by-step implementation process of the proposed adaptive HRA method. The procedural steps of the proposed method are summarized below (Fig. 4):

1. **Generate an initial set S_D of designs of experiment (DoE) sample points.**
   In this study, the Latin hypercube sampling (LHS) method is used for generating the DoE sample points, with an initial size determined as $N_0 = \max(10, 2+ N_x + N_y)$. The boundary values of the random variables are $[F_i^{-1}(\Phi(-5)), F_i^{-1}(\Phi(5))]$ $(i = 1, 2, \ldots, N_x)$, where F_i^{-1} is the inverse cumulative distribution function of $\boldsymbol{X}_i$. The boundary values of the interval variables are $[\boldsymbol{Y}^L, \boldsymbol{Y}^U]$. If a random variable $\boldsymbol{X}$ has a non-standard normal distribution, it needs to be transformed into a standard normal space using the Rosenblatt transformation.
2. **Construct the initial Kriging surrogate model.**
   For each sample point within the initial set S_D, the true performance function, $G(\boldsymbol{X}, \boldsymbol{Y})$, is evaluated to obtain the corresponding response values. These values compose an initial response set. Then, based on the sample point set and response set, construct the initial Kriging surrogate model. This model will serve as the foundation for subsequent adaptive learning processes.
3. **Computation of adaptive search space constraints.**
   This step marks the beginning of the iterative learning loop. At the start of each iteration, the dynamic search space must be redefined. The method, as described in Section 3.2.2, is used to compute the inner and outer constraint radii, β_1 and β_2, based on the current state of the Kriging model.

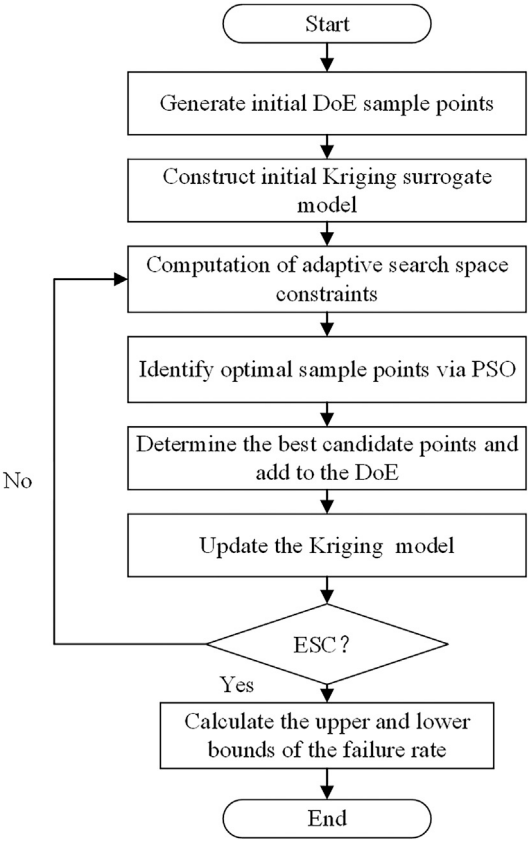

Fig. 4. Flowchart of the method.

4. **Identify optimal sampling points via PSO.**
   In this step, the next sample point $[X_{new}, Y_{new}]$ that most effectively improves the model accuracy is sought by solving a constrained optimization problem. This-problem aims to maximize the U learning function as the objective, subject to the multi-constraint system (including a dynamically constrained search space defined by β_1 and β_2, distance constraints, and truncated domain constraints) described in detail in Section 3. The PSO algorithm is then applied to globally solve this-problem, and the resulting point is identified as the new optimal sample point $[X_{new}, Y_{new}]$.
5. **Update the Kriging model.**
   The optimal sample point $[X_{new}, Y_{new}]$ identified is added to the experimental design sample point set S_D in step 4, and its response is evaluated by invoking the true LSF. Then, the Kriging model is retrained using the updated dataset to enhance its accuracy in approximating the true LSF.
6. **Convergence check.**
   After the model is updated, the ESC is calculated. The value of this criterion is then checked against the convergence condition defined in Eq. (36). If the condition is met, it signifies that the model's accuracy has reached the desired level. The learning process terminates, and the algorithm proceeds to the final reliability assessment. If the condition is not met, the algorithm returns to Step 4 to begin a new iteration of learning.
7. **Calculate the failure rate.**
   Once the algorithm has converged, the constructed Kriging model is used as a surrogate for the true LSF. The MCS method is then employed to calculate the upper and lower bounds of the failure probability. Specifically, for each Monte Carlo sample, an optimization algorithm is applied within the boundaries of interval variables to rapidly solve Eq. (3) and Eq. (4) using the final Kriging model, yielding extremal responses (G_{min} and G_{max}). The final probability bounds, P_f^{min} and P_f^{max}, are then determined by statistically aggregating the outcomes from all samples.

5. Numerical examples

To rigorously evaluate the precision, efficiency, and robustness of the proposed method, this-section applies it to five distinct numerical case studies encompassing scenarios ranging from mathematical functions to engineering problems. Our approach undergoes systematic performance comparisons with MCS and other advanced HRA methods. A detailed analysis of results is conducted to demonstrate the method's advantages in both computational cost and accuracy, thereby validating its effectiveness and practical applicability. Each experiment was independently executed 10 times to ensure statistical significance. The performance of the proposed method is verified through relative errors and the number of calls to the true performance function.

5.1. Example 1: a mathematical example

Two random variables and one interval variable are involved in this example. The definition of the performance function is [35,44]:

$$G(\boldsymbol{X}, \boldsymbol{Y}) = \sin\left(\frac{5x_1}{2}\right) - \frac{(x_1^2+4)(x_2-1)}{20} + y \tag{37}$$

where $x_1 \sim N(1.5, 1^2)$ and $x_2 \sim N(2.5, 1^2)$ are two independent normal random variables. For interval variables, two different cases are discussed here. Scenario 1: $y \in [2, 2.5]$ and Scenario 2: $y \in [4, 4.5]$. All methods used the LHS method to generate the 10 initial samples, and the failure probability bounds calculated using the MCS method are used as a benchmark for evaluating the superiority of other methods. N_{calls} indicates the quantity of calls to the real performance function; $\hat{p}_f^{\max}$ is the maximum failure rate and $\hat{p}_f^{\min}$ is the minimum failure rate; ε_1 and ε_2 represent the absolute relative errors of the maximum and minimum of the failure probability, respectively.

In Scenario 1, the failure probability boundaries determined by MCS lie within the range of 10^{-2} to 10^{-3}, representing a problem of moderate difficulty. As shown in Table 1, all advanced surrogate model methods exhibit commendable performance. The method proposed in this work achieves the highest efficiency with an average of 42.0 function evaluations (N_{calls}) while maintaining exceptional accuracy (ε_1 = 0.2274 %, ε_2 = 0.3218 %). These results demonstrate the initial validity of the method's effectiveness. The true test of the algorithm's capabilities materializes in Scenario 2. By adjusting interval variables, we rigorously narrow the problem into the rare-event domain, where the failure probability drops to the 10^{-4} magnitude. This sharp reduction underscores an intense challenge for the algorithm. Under this scenario, a dramatic divergence in the performance of the different methods is observed. The proposed method achieves high efficiency, requiring only 36.9 function evaluations (N_{calls}) to accurately complete the reliability assessment. This-value not only represents the lowest among all methods but also slightly surpasses its performance in the simpler Scenario 1. In stark contrast, other methods either suffer significant efficiency degradation (e.g., ALK-HRA's N_{calls} increases to 80.6) or sacrifice substantial accuracy to maintain efficiency (e.g., AK-MCS's ε_2 sharply rises to 7.0600 %). This clearly reveals the inherent difficulty of existing methods in balancing efficiency and accuracy when the LSS falls into the tail region of the probability distribution. Remarkably, the proposed method achieves a slight reduction in N_{calls} (to 36.9) even in the more complex Scenario 2. This seemingly paradoxical result directly validates the mechanistic superiority of its adaptive sampling strategy. The active learning strategy we employ exhibits strong sensitivity to information-rich regions. In rare-event problems, these regions inherently coincide with the tails of the probability density function. Therefore, the algorithm can lock onto the target more rapidly, ensuring that every function call is maximally effective, thus achieving faster convergence and avoiding excessive exploration in the more scattered, uncertain regions of moderate probability.

Table 1
Estimated results using different methods for Example 1.

	Method	N_{calls}	$\hat{p}_f^{\max}$	Cov_{max}(%)	ε_1(%)	$\hat{p}_f^{\min}$	Cov_{min}(%)	ε_2(%)
1	MCS	2×10^6	3.115×10^{-2}	–	–	5.905×10^{-3}	–	–
	AK-MCS	64.9	3.129×10^{-2}	1.760	0.4430	5.946×10^{-3}	4.090	0.6943
	ALK-HRA	70.4	3.105×10^{-2}	1.767	0.3274	5.898×10^{-3}	4.108	0.1185
	ALK-TCR-HRA	48.5	3.151×10^{-2}	2.099	1.1570	5.942×10^{-3}	4.900	0.6209
	proposed method	42.0	3.122×10^{-2}	1.792	0.2274	5.924×10^{-3}	4.098	0.3218
2	MCS	101×10^6	6.510×10^{-4}	–	–	2.900×10^{-4}	–	–
	AK-MCS	49.9	6.362×10^{-4}	3.208	2.2700	2.695×10^{-4}	4.929	7.0600
	ALK-HRA	80.6	6.470×10^{-4}	3.500	0.6100	2.850×10^{-4}	6.550	1.7200
	ALK-TCR-HRA	63.5	6.700×10^{-4}	3.270	2.9200	2.850×10^{-4}	6.470	1.7200
	proposed method	36.9	6.572×10^{-4}	3.274	0.9531	2.978×10^{-4}	4.865	2.6850

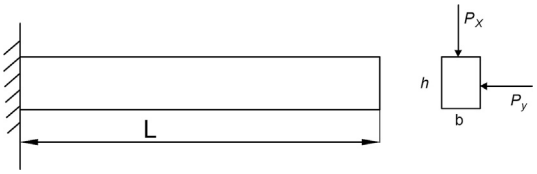

Fig. 5. Cantilever beam.

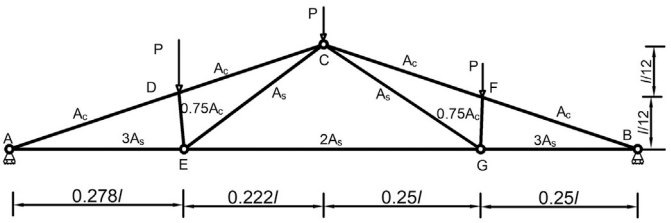

Fig. 6. Roof truss structure.

Table 2
Parameter information for Example 2.

Variable	Unit	Distribution type	Parameter 1	Parameter 2
L	mm	Normal	1000	100
b	mm	Normal	100	15
h	mm	Normal	200	20
P_x	N	Interval	47000	53000
P_y	N	Interval	23000	27000

5.2. Example 2: cantilever beam

There are three random variables and two interval variables in the cantilever beam structure shown in Fig. 5 [15]. The allowable stress of the material is $S = 370$ MPa. According to the principles of material mechanics, the maximum internal stress in a cantilever beam structure occurs at the fixed end. As the maximum stress cannot exceed the allowable stress, the structural performance function is derived as:

$$G(\boldsymbol{X},\boldsymbol{Y}) = S - \frac{6P_xL}{b^2h} - \frac{6P_yL}{bh^2} \tag{38}$$

where L, b and h are the length, width and height of the beam's cross-sectional area, respectively. P_x and P_y are the forces acting at the free end of the beam. Table 2 summarizes information on the uncertainty variables. For the random variables, the parameters 1 and 2 represent the mean and variance, respectively; for the interval variables, the parameters 1 and 2 represent the lower and upper bounds, respectively.

For this case, an initial Kriging surrogate model was constructed using 10 sample points, and the failure probability was calculated by averaging over 10 independent executions. As we can see in Table 3, the AK-MCS and ALK-HRA methods exhibit low computational efficiency, with high numbers of function evaluations required (95.2 and 92.1, respectively). The ALK-TCR-HRA method shows a significant improvement in efficiency compared to the first two methods; however, it remains less efficient than the proposed method. In terms of accuracy, the proposed method achieves relative errors of 0.2691 % and 0.9543 %, which are significantly lower than those of the ALK-TCR-HRA method. This demonstrates that the proposed method, by optimizing the selection of training sample points and employing the ESC, not only identifies optimal training points accurately but also avoids unnecessary training points while maintaining high precision.

Table 4
Parameter information for Example 3.

Variable	Unit	Distribution type	Parameter 1	Parameter 2
q	N/m	Normal	20000	1600
l	m	Normal	12	0.24
E_s	N/m^2	Normal	1.2×10^{11}	8.4×10^{9}
E_c	N/m^2	Normal	3×10^{10}	2.4×10^{9}
A_s	m^2	Interval	9.3×10^{-4}	9.5×10^{-4}
A_c	m^2	Interval	0.033	0.035

5.3. Example 3: roof truss structure

The roof truss structure model is examined as a case study to further demonstrate the effectiveness of the proposed approach [33,36]. As illustrated in Fig. 6, the structure consists of two interval variables and four random variables. The top of the roof and the compression members are reinforced with concrete, while the bottom and the tie rods are manufactured from steel. The load q on the roof is uniformly distributed, and this load is converted into equivalent nodal loads $P = ql/4$ at nodes C, D and F. The performance function is expressed using the analytical vertical deflection formula at node C:

$$G(\boldsymbol{X},\boldsymbol{Y}) = \Delta - \frac{ql^2}{2}\left(\frac{3.81}{A_cE_c} + \frac{1.13}{A_sE_s}\right) \tag{39}$$

where E_c and E_s are the elastic moduli of these materials. A_c and A_s are the concrete and steel cross-sectional areas, respectively. At node C, the maximum vertical deflection is 0.025 m. Table 4 presents the uncertainty information for the relevant parameters.

In terms of computational efficiency, it can be seen from Table 5 that the N_{calls} by the proposed method is 25.4, compared to 97.5, 89.9 and 33.2 for the AK-MCS, ALK-HRA and ALK-TCR-HRA methods, respectively. Obviously, the quantity of function evaluations is significantly reduced by the proposed method. Regarding computational accuracy, the results using the MCS are 1.840×10^{-2} and 8.310×10^{-3}. In comparison, the proposed method yields bounds of 1.846×10^{-2} and 8.361×10^{-3}, with ε_1 and ε_2 being 0.3207 % and 0.6137 %, respectively. The AK-MCS method produces bounds of 1.845×10^{-2} and 8.409×10^{-3}, with ε_1 and ε_2 being 0.2554 % and 1.1910 %, respectively. The ALK-HRA method results in bounds of 1.836×10^{-2}, 8.330×10^{-3}, with ε_1 being 0.2120 % and ε_2 being 0.2407 %. Finally, the ALK-TCR-HRA method gives bounds of 1.895×10^{-2}, 8.568×10^{-3}, with ε_1 and ε_2 being 2.9670 % and 3.1050 %, respectively. These results indicate that although both ALK-TCR-HRA

Table 3
Estimated results using different methods for Example 2.

Method	N_{calls}	$\hat{p}_f^{\max}$	Cov_{max}(%)	ε_1(%)	$\hat{p}_f^{\min}$	Cov_{min}(%)	ε_2(%)
MCS	2×10^6	4.041×10^{-2}	–	–	1.970×10^{-3}	–	–
AK-MCS	95.2	4.017×10^{-2}	1.546	0.5840	1.974×10^{-3}	2.229	0.2132
ALK-HRA	92.1	4.016×10^{-2}	1.546	0.6137	1.974×10^{-3}	2.229	0.2203
ALK-TCR-HRA	47.6	4.192×10^{-2}	3.199	3.7330	2.038×10^{-3}	4.630	3.4430
proposed method	42.9	4.052×10^{-2}	1.539	0.2691	1.951×10^{-3}	2.242	0.9543

Table 5
Estimated results using different methods for Example 3.

Method	N_{calls}	$\hat{p}_f^{\max}$	Cov_{max}(%)	ε_1(%)	$\hat{p}_f^{\min}$	Cov_{min}(%)	ε_2(%)
MCS	2×10^6	1.840×10^{-2}	–	–	8.310×10^{-3}	–	–
AK-MCS	97.5	1.845×10^{-2}	2.307	0.2554	8.409×10^{-3}	3.435	1.1910
ALK-HRA	89.9	1.836×10^{-2}	2.313	0.2120	8.330×10^{-3}	3.452	0.2407
ALK-TCR-HRA	33.2	1.895×10^{-2}	3.220	2.9670	8.568×10^{-3}	4.816	3.1050
proposed method	25.4	1.846×10^{-2}	2.309	0.3207	8.361×10^{-3}	3.447	0.6137

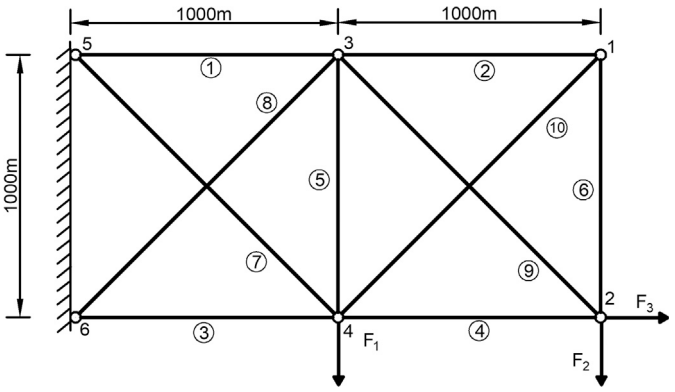

Fig. 7. Ten-bar truss.

Table 6
Parameter information for Example 4.

Variable	Unit	Distribution type	Parameter 1	Parameter 2
A_1	mm^2	Normal	1000	50
A_2	mm^2	Normal	1000	50
A_3	mm^2	Normal	1000	50
F_1	kN	Interval	79.5	80.5
F_2	kN	Interval	79.5	80.5
F_3	kN	Interval	9.9	10.1

method and the proposed method significantly reduce the number of function evaluations, the ALK-TCR-HRA method sacrifices accuracy to a certain extent. In contrast, the proposed method achieves high computational efficiency while keeping the relative errors at less than 1 % for both failure probability bounds.

5.4. Example 4: ten-bar truss

As an engineering case study, this-section analyzes a ten-bar truss structure [35]. The structure consists of three interval variables and three random variables, as shown in Fig. 7. The cross-sectional areas of members 1–4, 5–6 and 7–10 are denoted as A_1, A_2 and A_3, respectively. Vertical load F_1 acts on node 4, whereas node 2 experiences the application of both horizontal load F_3 and vertical load F_2. The elastic modulus E is 1×10^5 MPa. The statistical distribution is provided in Table 6, where random variables A_1, A_2 and A_3 follow normal distributions, and F_1, F_2 and F_3 are interval variables.

The allowable limit for vertical displacement at node 2 is set at 9.3 mm. Thus, the definition of a performance function is:

$$G(\boldsymbol{X}, \boldsymbol{Y}) = 9.3 - \Delta \tag{40}$$

Table 7 presents the comparative results. The results using the MCS are 1.970×10^{-2}, 8.350×10^{-3}. The AK-MCS and ALK-HRA methods require 81.4 and 73.3 function evaluations, respectively, to achieve convergence. The ALK-TCR-HRA method requires 30.2 function evaluations and produces failure probability bounds of 2.028×10^{-2} and 8.345×10^{-3}. The the maximum relative error ε_1 of 2.9510 % is the maximum of any method, and the minimum relative error ε_2 of 0.0599 % is the minimum. This indicates that the ALK-TCR-HRA method is less accurate in simultaneously computing the failure probability.

In contrast, the proposed method requires the fewest function evaluations (22.7) while demonstrating excellent computational accuracy, with relative errors for the failure probability bounds remaining around 1 %. These results highlight the superior efficiency and precision of the proposed method.

Table 7
Estimated results using different methods for Example 4.

Method	N_{calls}	$\hat{p}_f^{max}$	Cov_{max}(%)	ε_1(%)	$\hat{p}_f^{min}$	Cov_{min}(%)	ε_2(%)
MCS	2×10^6	1.970×10^{-2}	–	–	8.350×10^{-3}	–	–
AK-MCS	81.4	1.976×10^{-2}	2.228	0.2944	8.259×10^{-3}	3.466	1.0900
ALK-HRA	73.3	1.984×10^{-2}	2.223	0.7107	8.202×10^{-3}	3.478	1.7720
ALK-TCR-HRA	30.2	2.028×10^{-2}	3.083	2.9510	8.345×10^{-3}	4.834	0.0599
proposed method	22.7	1.991×10^{-2}	2.219	1.0610	8.270×10^{-3}	3.364	0.9581

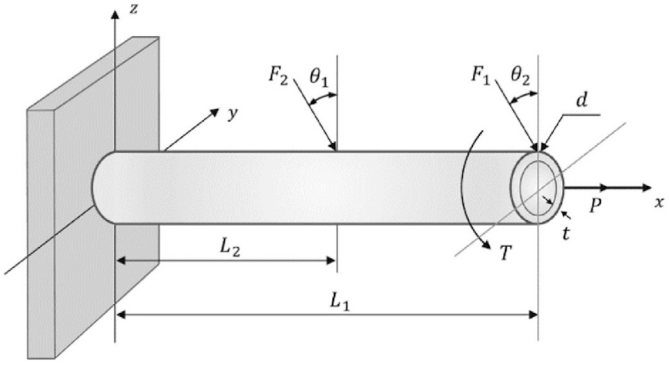

Fig. 8. Cantilever tube.

5.5. Example 5: cantilever tube

In order to evaluate the performance of the proposed method in high-dimensional problems, a cantilever tube structure is analyzed, as shown in Fig. 8. The external forces F_1, F_2, P and a torque T act on the cantilever. Failure occurs when the maximum stress $\sigma_{\max}$ at the top of the cantilever tube at the origin exceeds the material's yield limit S_y. The limit state function is defined as [35,44]:

$$G(\boldsymbol{X}, \boldsymbol{Y}) = S_y - \sigma_{\max} = S_y - \sqrt{\sigma_x^2 + 3\tau_{zx}^2} \tag{41}$$

where σ_x represents the normal stress at the origin, given as:

$$\sigma_x = \frac{P + F_1 \sin(\theta_1) + F_2 \sin(\theta_2)}{A} + \frac{Md}{2I} \tag{42}$$

where the first term denotes the axial stress due to the axial force, $A = \frac{\pi}{4}\left[d^2 - d(d-2t)^2\right]$, whereas the second term represents the bending stress due to the moment, $I = \frac{\pi}{64}\left[d^4 - d(d-2t)^4\right]$, $M = F_1 L_1 \cos(\theta_1) + F_2 L_2 \cos(\theta_2)$. L_1 represents the total length of the cantilever tube; L_2 is the distance from the fixed end to where force F_2 is applied; d and t are the outer diameter and wall thickness of the tube, respectively; θ_1 and θ_2 are the application angles of forces F_2 and F_1. The shear stress at the origin τ_{zx} is given by:

$$\tau_{zx} = \frac{Td}{2J} \tag{43}$$

where $J = 2I$.

This example involves 11 variables, including 7 random variables and 4 interval variables, with their information provided in Table 8. For all methods, the initial sample size used to construct the Kriging model is set to 13. As shown in Table 9, the number of function evaluations required by the four methods is 200.5 (AK-MCS), 173.8 (ALK-HRA), 73.50 (ALK-TCR-HRA) and 26.50 (proposed method). Evidently, the proposed method significantly reduces the number of function evaluations in this high-dimensional case, demonstrating substantial improvements in computational efficiency.

In terms of accuracy, the results using the MCS are 1.816×10^{-2} and 1.356×10^{-2}. The proposed method yields bounds of 1.815×10^{-2}

Table 8
Parameter information for Example 5.

Variable	Unit	Distribution type	Parameter 1	Parameter 2
t	mm	Normal	5	0.1
d	mm	Normal	42	0.5
P	kN	Normal	12	1.2
F_1	kN	Normal	3	0.3
F_2	kN	Normal	3	0.3
T	N · mm	Normal	90	9
S_y	MPa	Normal	180	22
L_1	mm	Interval	59.75	60.25
L_2	mm	Interval	119.75	120.25
θ_1	deg	Interval	0	10
θ_2	deg	Interval	5	15

Table 9
Estimated results using different methods for Example 5.

Method	N_{calls}	$\hat{p}_f^{\max}$	Cov_{max}(%)	ε_1(%)	$\hat{p}_f^{\min}$	Cov_{min}(%)	ε_2(%)
MCS	2×10^6	1.816×10^{-2}	–	–	1.356×10^{-3}	–	–
AK-MCS	200.5	1.877×10^{-2}	2.286	3.3810	1.412×10^{-3}	2.643	4.1150
ALK-HRA	173.8	1.869×10^{-2}	2.292	2.9240	1.419×10^{-3}	2.636	4.6170
ALK-TCR-HRA	73.50	1.872×10^{-2}	4.127	3.0790	1.415×10^{-3}	4.757	4.3820
proposed method	26.50	1.815×10^{-2}	2.328	0.0606	1.373×10^{-3}	2.682	1.2390

and 1.373×10^{-2}, with relative errors ε_1 and ε_2 of 0.0606 % and 1.2390 %, respectively. As shown in Table 9, the proposed method achieves the smallest relative errors for both failure probability bounds. For the case studied, the proposed method demonstrates encouraging computational efficiency and accuracy compared to the other methods. This highlights its potential for addressing problems of moderate-to-high dimensionality.

6. Conclusion

This study has proposed and validated a novel global adaptive learning strategy for hybrid reliability analysis. This-section summarizes the method's core contributions, its performance, and future research directions.

Focusing on reliability problems involving both random and interval uncertainties, this study presents a new active learning analysis method based on Kriging surrogate modeling. The core innovation lies in establishing a completely new adaptive learning framework that eliminates dependence on candidate sample pools. By deeply integrating the U learning function with the PSO algorithm, the framework achieves global dynamic search for optimal update sample points. In each iteration, the PSO maximizes the U learning function as its objective, searching within a dynamically adjusted space. This search space is governed by a multi-constraint system, including two boundary constraints, a distance constraint, and a global domain truncation constraint. This intelligent optimization strategy, which integrates multiple constraints with the global search capability of PSO, completely eliminates the dependence of traditional methods on a pre-defined candidate sample pool, thereby enabling a more efficient convergence to the true limit state boundary. The entire iterative process is monitored by an extended ESC to ensure efficient termination after achieving the target accuracy.

The performance of the proposed method was systematically validated through five numerical examples, including benchmark mathematical functions and engineering applications. Comparative studies against established methods such as MCS, AK-MCS, ALK-HRA, and ALK-TCR-HRA demonstrated the effectiveness of our approach. The results confirm that the proposed method achieves a more effective balance between computational accuracy and efficiency, significantly reducing the number of calls to the expensive limit state function while maintaining a high level of precision in estimating the bounds of failure probability.

Although the proposed method has achieved encouraging results for the static reliability problems investigated, we recognize that its applicability to more complex scenarios requires further exploration. Future research will primarily focus on the following two directions: First, the extension of the method to high-dimensional problems. The validation in this paper was mainly concentrated on low- to moderate-dimensional problems. As the dimensionality of design variables increases significantly, both the construction cost of the Kriging model and the search efficiency of the optimization algorithm will face the severe challenge of the "curse of dimensionality." Therefore, investigating how to combine the current framework with dimensionality reduction techniques (e.g., Principal Component Analysis) or advanced high-dimensional surrogate modeling techniques(e.g., sparse grids or polynomial chaos expansions) is a critical step to enhance the method's practical utility and represents a primary focus of our future work. Second, the application of the method to time-variant reliability analysis. The present study primarily considered cases where uncertainty parameters do not change over time. However, in many real-world engineering problems, factors such as material degradation and load variations cause structural performance to degrade over time, which is a typical time-variant reliability problem. How to integrate the active learning strategy proposed herein with stochastic process theory to efficiently predict the failure probability over a structure's entire lifecycle is a research direction of significant theoretical value and engineering importance.

CRediT authorship contribution statement

Cheng Yang: Writing – original draft, Validation, Software, Methodology, Data curation. **Qingwei Liang:** Methodology, Funding acquisition, Conceptualization. **Hancheng Huang:** Software, Funding acquisition. **Enrico Zio:** Writing – review & editing. **Yuxin Lin:** Data curation. **Shanshan Hu:** Writing – review & editing.

Replication of results

Detailed procedures and flowchart of the proposed algorithm have been presented in Section 4 and one can follow them to reproduce the results. The author will assist interested researchers in reproducing the results in this paper except for the simulation case in Section 5.

Declaration of competing interest

The authors declare that they have no known competing financial interests or personal relationships that could have appeared to influence the work reported in this paper.

Funding

The authors are grateful for the Natural Science Basic Research Program of Shaanxi (No.2024JC-YBMS-790), the Program of China Scholarship Council (Grant No.202306290130) and the Innovation Foundation for Doctoral Dissertation of Northwestern Polytechnical University (Grant No.CX2024047).

Data availability

The authors do not have permission to share data.

References

[1] Li P, Wang Y. An active learning reliability analysis method using adaptive bayesian compressive sensing and monte carlo simulation (abcs-mcs). Reliab Eng Syst Saf 2022 May;221:108377. https://doi.org/10.1016/j.ress.2022.108377
[2] Pan Q, Dias D. An efficient reliability method combining adaptive support vector machine and monte carlo simulation. Structural Safety 2017;67:85–95. https://doi.org/10.1016/j.strusafe.2017.04.006
[3] Arab HG, Rashki M, Rostamian M, Ghavidel A, Shahraki H, Keshtegar B. Refined first-order reliability method using cross-entropy optimization method. Eng Comput 2019;35(4):1507–19. https://doi.org/10.1007/s00366-018-0680-9
[4] Zhong C, Wang M, Dang C, Ke W. Structural reliability assessment by salp swarm algorithm-based form. Qual Reliab Eng Int 2020;36(4):1224–44. https://doi.org/10.1002/qre.2626

[5] Lim J, Lee B, Lee I. Second-order reliability method-based inverse reliability analysis using hessian update for accurate and efficient reliability-based design optimization. Int J Numer Methods Eng 2014;100(10):773–92. https://doi.org/10.1002/nme.4775
[6] Bichon BJ, Eldred MS, Swiler LP, Mahadevan S, McFarland JM. Efficient global reliability analysis for nonlinear implicit performance functions. Aiaa J 2008;46(10):2459–68. https://doi.org/10.2514/1.34321
[7] Echard B, Gayton N, Lemaire M. Ak-mcs: an active learning reliability method combining kriging and monte carlo simulation. Structural Safety 2011;33(2):145–54. https://doi.org/10.1016/j.strusafe.2011.01.002
[8] Lv Z, Lu Z, Wang P. A new learning function for kriging and its applications to solve reliability problems in engineering. Comput Math Appl 2015;70(5):1182–97. https://doi.org/10.1016/j.camwa.2015.07.004
[9] Yang S, Meng D, Wang H, Yang C. A novel learning function for adaptive surrogate-model-based reliability evaluation. Philos Trans R Soc A Math Phys Eng Sci 2024 JAN 8;382(2264). https://doi.org/10.1098/rsta.2022.0395
[10] Zhang X, Wang L, Sorensen JD. Reif: a novel active-learning function toward adaptive kriging surrogate models for structural reliability analysis. Reliab Eng Syst Saf 2019;185:440–54. https://doi.org/10.1016/j.ress.2019.01.014
[11] Cai Y, Zhao W, Wang X, Ou Y, Chen Y, Li X. A novel multiple linearization method for reliability analysis based on evidence theory. Reliab Eng Syst Saf 2024;250:110278. https://doi.org/10.1016/j.ress.2024.110278. https://www.sciencedirect.com/science/article/pii/S0951832024003508
[12] Zhang D, Hao Z, Han X, Dai S, Li Q. A new probabilistic transformation technique for evidence-theory-based structural reliability analysis. Reliab Eng Syst Saf 2025;258:110891. https://doi.org/10.1016/j.ress.2025.110891. https://www.sciencedirect.com/science/article/pii/S0951832025000948
[13] Zhang Z, Jiang C. Evidence-theory-based structural reliability analysis with epistemic uncertainty: a review. Struct Multidiscip Optim 2021;63(6):2935–53. https://doi.org/10.1007/s00158-021-02863-w
[14] Wang L, Liu J. Dynamic uncertainty quantification and risk prediction based on the grey mathematics and outcrossing theory. Appl Sci (switzerland) 2022;12(11):5389. https://doi.org/10.3390/app12115389
[15] Hong L, Li H, Gao N, Fu J, Peng K. Random and multi-super-ellipsoidal variables hybrid reliability analysis based on a novel active learning kriging model. Comput Methods Appl Mech Eng 2021;373:113555. https://doi.org/10.1016/j.cma.2020.113555. https://www.sciencedirect.com/science/article/pii/S0045782520307404
[16] Zhou C, Xiao N-C, Zuo MJ, Gao W. An active kriging-based learning method for hybrid reliability analysis. IEEE Trans Reliab 2022;71(4):1567–76. https://doi.org/10.1109/TR.2021.3111926
[17] Wang T, Yang X, Mi C. An efficient hybrid reliability analysis method based on active learning kriging model and multimodal-optimization-based importance sampling. Int J Numer Methods Eng 2021;122(24):7664–82. https://doi.org/10.1002/nme.6847
[18] Dong B, Lu Z. An efficient estimation of failure probability in the presence of random and interval hybrid uncertainty. Struct Multidiscip Optim 2021;63(6):2613–35. https://doi.org/10.1007/s00158-021-02867-6
[19] Wang G, Monaghan M, Zhang M. Parallelizing adaptive reliability analysis through penalizing the learning function. IEEE Trans Reliab 2024:1–15. https://doi.org/10.1109/TR.2024.3483307
[20] Che Y, Ma Y, Li Y, Ouyang L. A novel active-learning kriging reliability analysis method based on parallelized sampling considering budget allocation. IEEE Trans Reliab 2024;73(1):589–601. https://doi.org/10.1109/TR.2023.3311192
[21] Du X. Unified uncertainty analysis by the first order reliability method. J Mech Des 2008;130(9):0914011–09140110. https://doi.org/10.1115/1.2943295
[22] Xiao NC, Huang HZ, Wang Z, Liu Y, Zhang XL. Unified uncertainty analysis by the mean value first order saddlepoint approximation. Struct Multidiscip Optim 2012;46(6):803–12. https://doi.org/10.1007/s00158-012-0794-4
[23] Luo C, Zhu S-P, Keshtegar B, Macek W, Branco R, Meng D. Active kriging-based conjugate first-order reliability method for highly efficient structural reliability analysis using resample strategy. Comput Methods Appl Mech Eng 2024;423:116863. https://doi.org/10.1016/j.cma.2024.116863. https://www.sciencedirect.com/science/article/pii/S0045782524001191
[24] Wang J, Lu Z. An efficient surrogate model method considering the candidate sample pool reduction by safety optimal hypersphere for random-interval mixed reliability analysis. Eng Comput 2024;40(2):795–811. https://doi.org/10.1007/s00366-023-01815-w
[25] Wang D, Zhang D, Meng Y, Yang M, Meng C, Han X, et al. Ak-hrn: an efficient adaptive kriging-based n-hypersphere rings method for structural reliability analysis. Comput Methods Appl Mech Eng 2023;414:116146. https://doi.org/10.1016/j.cma.2023.116146. https://www.sciencedirect.com/science/article/pii/S0045782523002700
[26] Shen C, Ruan X, Liu T, Xu M, Li P. A dimension-wise analysis driven active learning paired-kriging (DWA-ALK) method for the hybrid reliability analysis. Structures 2023;47(December 2022):939–52. https://doi.org/10.1016/j.istruc.2022.11.108
[27] Xiao T, Park C, Lin C, Ouyang L, Ma Y. Hybrid reliability analysis with incomplete interval data based on adaptive kriging. Reliab Eng Syst Saf 2023;237(August 2022):109362. https://doi.org/10.1016/j.ress.2023.109362
[28] Wang J, Lu Z, Wang L. An efficient method for estimating failure probability bounds under random-interval mixed uncertainties byÂ combining line sampling with adaptive kriging. Int J Numer Methods Eng 2023;124(2):308–33. https://doi.org/10.1002/nme.7122
[29] Thedy J, Liao KW. Adaptive kriging adopting PSO with hollow-hypersphere space in structural reliability assessment. Probabilist Eng Mech 2023;74(March):103513. https://doi.org/10.1016/j.probengmech.2023.103513
[30] Ye N, Lu Z, Zhang X, Feng K. Metamodel-based directional importance sampling for structural reliability analysis. IEEE Trans Reliab 2024;73(1):463–77. https://doi.org/10.1109/TR.2023.3294336
[31] Yang X, Liu Y, Gao Y, Zhang Y, Gao Z. An active learning kriging model for hybrid reliability analysis with both random and interval variables. Struct Multidiscip Optim 2015;51(5):1003–16. https://doi.org/10.1007/s00158-014-1189-5
[32] Zhang J, Xiao M, Gao L, Fu J. A novel projection outline based active learning method and its combination with kriging metamodel for hybrid reliability analysis with random and interval variables. Comput Methods Appl Mech Eng 2018;341:32–52. https://doi.org/10.1016/j.cma.2018.06.032
[33] Zhang J, Xiao M, Gao L, Chu S. A combined projection-outline-based active learning Kriging and adaptive importance sampling method for hybrid reliability analysis with small failure probabilities. Comput Methods Appl Mech Eng 2019;344:13–33. https://doi.org/10.1016/j.cma.2018.10.003
[34] Zhang J, Gao L, Xiao M. A composite-projection-outline-based approximation method for system reliability analysis with hybrid uncertainties. Reliab Eng Syst Saf 2020;204(August):107169. https://doi.org/10.1016/j.ress.2020.107169
[35] Yang X, Wang T, Li J, Chen Z. Bounds approximation of limit-state surface based on active learning kriging model with truncated candidate region for random-interval hybrid reliability analysis. Int J Numer Methods Eng 2020;121(7):1345–66. https://doi.org/10.1002/nme.6269
[36] Xiao M, Zhang J, Gao L, Lee S, Eshghi AT. An efficient kriging-based subset simulation method for hybrid reliability analysis under random and interval variables with small failure probability. Struct Multidiscip Optim 2019;59(6):2077–92. https://doi.org/10.1007/s00158-018-2176-z
[37] Zhao Z, Lu ZH, Zhao YG, Xu TF, Zhang YF. A novel random-interval hybrid reliability analysis method combining active learning Kriging and two-phase subset simulation. Structures 2024;63(March):106383. https://doi.org/10.1016/j.istruc.2024.106383
[38] Lataniotis C, Wicaksono D, Marelli S, Sudret B. Uqlab user manual – kriging (gaussian process modeling), Tech. rep., Chair of Risk, Safety and Uncertainty Quantification, ETH Zurich, Switzerland, report UQLab-V2.1-105 (2024).
[39] Wang Y, Pan H, Shi Y, Wang R, Wang P. A new active-learning estimation method for the failure probability of structural reliability based on kriging model and simple penalty function. Comput Methods Appl Mech Eng 2023;410:116035. https://doi.org/10.1016/j.cma.2023.116035
[40] Kim J, Song J. Probability-adaptive kriging in n-ball (PAK-Bn) for reliability analysis. Structural Safety 2020;85(January):101924. https://doi.org/10.1016/j.strusafe.2020.101924
[41] Wang J, Xu G, Li Y, Kareem A. AKSE: a novel adaptive kriging method combining sampling region scheme and error-based stopping criterion for structural reliability analysis. Reliab Eng Syst Saf 2022;219(November 2021):108–214. 10.1016/j.ress.2021.108214
[42] Wang Z, Shafieezadeh A. ESC: an efficient error-based stopping criterion for kriging-based reliability analysis methods. Struct Multidiscip Optim 2019;59(5):1621–37. https://doi.org/10.1007/s00158-018-2150-9
[43] Wang J, Xu G, Yuan P, Li Y, Kareem A. An efficient and versatile kriging-based active learning method for structural reliability analysis. Reliab Eng Syst Saf 2024;241(September 2022):109670. https://doi.org/10.1016/j.ress.2023.109670
[44] Zhou C, Xiao NC, Zuo MJ, Gao W. An active kriging-based learning method for hybrid reliability analysis. IEEE Trans Reliab 2022;71(4):1567–76. https://doi.org/10.1109/TR.2021.3111926